

# UC Riverside

## UC Riverside Previously Published Works

### Title

Examining the Potential for Methyl Halide Accumulation and Detectability in Possible Hycean-type Atmospheres

### Permalink

<https://escholarship.org/uc/item/4pr6w862>

### Journal

The Astrophysical Journal Letters, 982(1)

### ISSN

2041-8205

### Authors

Leung, Michaela

Tsai, Shang-Min

Schwieterman, Edward W

et al.

### Publication Date

2025-03-20

### DOI

10.3847/2041-8213/adb558


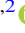



### Copyright Information

This work is made available under the terms of a Creative Commons Attribution License, available at <https://creativecommons.org/licenses/by/4.0/>

Peer reviewed



# Examining the Potential for Methyl Halide Accumulation and Detectability in Possible Hycean-type Atmospheres

Michaela Leung<sup>1,2</sup> , Shang-Min Tsai<sup>1,2</sup> , Edward W. Schwieterman<sup>1,3</sup> , Daniel Angerhausen<sup>3,4</sup> , and Janina Hansen<sup>4</sup> 

<sup>1</sup>Department of Earth and Planetary Sciences, University of California, Riverside, CA 92521, USA; [michaela.leung@email.ucr.edu](mailto:michaela.leung@email.ucr.edu)

<sup>2</sup>NASA Alternative Earths Team, USA

<sup>3</sup>Blue Marble Space Institute of Science, Seattle, WA, USA

<sup>4</sup>ETH Zurich, Institute for Particle Physics & Astrophysics, Wolfgang-Pauli-Str. 27, 8093 Zurich, Switzerland

Received 2024 November 27; revised 2025 January 31; accepted 2025 February 12; published 2025 March 11

## Abstract

Some sub-Neptune planets may host habitable conditions; for example “Hycean” worlds with H<sub>2</sub> envelopes over liquid water oceans can maintain potentially hospitable pressures and temperatures at their surface. Recent JWST observations of K2-18b and TOI-270d have shown that such worlds could be compelling targets for biosignature searches, given their extended scale heights and therefore large atmospheric signatures. Methylated biosignatures, a broad group of gases that can be generated by biological attachment of a CH<sub>3</sub> group to an environmental substrate, have been proposed as candidate signs of life for Earth-like exoplanets. However, methyl halides (CH<sub>3</sub> + halogen) have not yet been robustly examined with self-consistent photochemical and spectral models for planets with H<sub>2</sub>-dominated atmospheres. Here we demonstrate that methyl chloride (CH<sub>3</sub>Cl), predominantly produced by marine microbes, could be detected using JWST in tens of transits or fewer for Hycean planets, comparable to detection requirements for other potential atmospheric biosignatures. The threshold atmospheric mixing ratio for detectability is ~10 ppm, which can accumulate with global fluxes comparable to moderately productive local environments on Earth.

*Unified Astronomy Thesaurus concepts:* [Exoplanet atmospheres \(487\)](#); [Exoplanet atmospheric composition \(2021\)](#); [Biosignatures \(2018\)](#); [Astrobiology \(74\)](#)

## 1. Introduction

The search for life beyond the Earth is a compelling motivation to develop observational and modeling tools to characterize sub-Neptune and smaller exoplanets with high fidelity. Instrumental constraints have until recently limited this speculative area to preparatory modeling work, influenced by the planetary mass, radius, and distribution information gathered by survey missions such as Kepler (i.e., S. Greiss et al. 2012a, 2012b) and TESS (i.e., S. Sharma et al. 2017; N. M. Guerrero et al. 2021). These missions have revolutionized our statistical understanding of the exoplanet population, revealing the high frequency of “sub-Neptune” planets that exist between the radii of terrestrial Earth-like and gaseous Neptune-like planets (i.e., E. J. Rivera et al. 2005; D. Valencia et al. 2007; G. J. Bergsten et al. 2022). Substantial theoretical attention has been applied to these planets and their conditions, including their potential habitability (i.e., W. von Bloh et al. 2009; R. Hu et al. 2019; R. Claudi et al. 2020). A well-explored conception of these planets as conventionally habitable invokes an H<sub>2</sub>-rich atmosphere above a surface liquid water ocean, accommodating the reported mass and radius measurements and supporting a potentially hospitable ocean (N. Madhusudhan et al. 2021).

While some temperate sub-Neptune planets may support habitable (Hycean) conditions, this prediction is still being tested against observational data. Preliminary observations with JWST are degenerate with multiple atmospheric models that fit the limited data, including those that preclude habitable environments (A. Biagini et al. 2024; M. Damiano et al. 2024). It is

difficult to differentiate between plausible scenarios suggested by interior and atmospheric models (i.e., N. Madhusudhan et al. 2020), especially without a corresponding analog in our solar system. One method of distinguishing a massive envelope from a shallow habitable condition relies on differential solubility and photochemical lifetimes of key molecules in extended atmospheres (R. Hu et al. 2021; S.-M. Tsai et al. 2021a; X. Yu et al. 2021; Z. Huang et al. 2024; N. F. Wogan et al. 2024). The atmospheric presence of highly water-soluble molecules such as NH<sub>3</sub> or HCN could point to a dry or nonexistent surface, while the absence of these molecules and relative abundances of CH<sub>4</sub>, CO<sub>2</sub>, H<sub>2</sub>O, and C<sub>2</sub>H<sub>6</sub> could suggest the planet is Hycean in nature. Other techniques such as comparing the CO<sub>2</sub>-to-CH<sub>4</sub> ratio have also been proposed to probe the interior of planets in this size regime (J. Yang & R. Hu 2024).

Examinations of temperate sub-Neptune planets have been among the first rounds of observations made with JWST, including TOI-270d (B. Benneke et al. 2024; M. Holmberg & N. Madhusudhan 2024), LHS 1140b (A. Biagini et al. 2024; M. Damiano et al. 2024), and TOI-732b (S. H. C. Cabot et al. 2024). One well-known example is the planet K2-18b, a sub-Neptune target that was previously observed with the Hubble Space Telescope, producing the first claimed water detection on a sub-Neptune-sized planet (B. Benneke et al. 2019). However, this claim has been disputed, and the H<sub>2</sub>O features have been reinterpreted as CH<sub>4</sub> (N. Madhusudhan et al. 2023a). JWST observations of K2-18b (N. Madhusudhan et al. 2023b) reported the presence of both CO<sub>2</sub> and CH<sub>4</sub>. Coupled with the lack of CO and NH<sub>3</sub>, the authors argue that this atmospheric configuration is indicative of a Hycean planet. Additionally, N. Madhusudhan et al. (2023b) reported a tentative detection of dimethylsulfide (DMS; (CH<sub>3</sub>)<sub>2</sub>S), a candidate atmospheric biosignature, originally proposed by C. B. Pilcher (2003) and



Original content from this work may be used under the terms of the [Creative Commons Attribution 4.0 licence](#). Any further distribution of this work must maintain attribution to the author(s) and the title of the work, journal citation and DOI.

quantitatively studied in anoxic terrestrial atmospheres by S. D. Domagal-Goldman et al. (2011). However, this interpretation is far from unanimous, with challenges and alternative interpretations of the potential biosignature presented in the literature. These include the possibility that thick atmosphere scenarios may better fit the data and that  $\text{CH}_4$  absorption at the wavelength reported may overprint any potential DMS signal (S.-M. Tsai et al. 2024; N. F. Wogan et al. 2024). Some of these alternative models would indicate that K2-18b may be too hot to support a Hycean-type atmosphere, with proposed compositions ranging from magma ocean to thick greenhouse atmospheres (J. Leconte et al. 2024; O. Shorttle et al. 2024). These substitute theories have been challenged in turn, showing that there is yet little consensus on the nature of this planet (G. J. Cooke & N. Madhusudhan 2024; F. E. Rigby & N. Madhusudhan 2024). Regardless of whether further observations confirm the Hycean nature of K2-18b, the general question of biosignatures in Hycean worlds has been brought to the forefront of the scientific community and remains an interesting opportunity given the accessibility of these targets to JWST. For example, compositionally similar planets receiving lower incident stellar flux may be amenable to Hycean conditions even if K2-18b in particular does not host a temperate liquid water ocean.

S.-M. Tsai et al. (2024) used photochemical and spectral models to perform vertically integrated simulations of the survivability and detectability of biogenic sulfur gases (including candidate methylated biosignature DMS) in the atmosphere of K2-18b as a stand-in for Hycean worlds in general. This study found that for DMS to reach detectable levels a biological production flux of  $\sim 20$  times the globally averaged modern Earth flux is necessary. The authors applied both a 1D and 2D photochemical model and found that there is little difference between the simulated DMS outcomes, indicating that there is sufficient horizontal mixing in this case to oppose accumulation on the tidally locked nightside. Simulated spectra suggest that for NIRSpec wavelengths, DMS features are difficult to disentangle from  $\text{CH}_4$  with a cleaner feature accessible at mid-infrared wavelengths centered near  $\sim 10 \mu\text{m}$ .

DMS is a possible biosignature on Hycean worlds (N. Madhusudhan et al. 2023b; S.-M. Tsai et al. 2024) because the gas is formed via biological methylation of environmental substrates, a process that also generates other biogenic gases on Earth. Its origin is overwhelmingly biological on Earth. In addition to DMS, other methylated chalcogens (S, Se, Te), halogens (Cl, Br, I), and metal(loid) compounds have been examined or proposed as potential astronomical biosignatures (A. Segura et al. 2005; M. Leung et al. 2022; V. S. Meadows et al. 2023; E. W. Schwieterman & M. Leung 2024). Numerous clades of bacteria and algae are known to produce these methylated gases (i.e., K. R. Redeker et al. 2000; C. H. Dimmer et al. 2001; A. Shibasaki et al. 2016). Depending on host star and production rate (surface flux), some of these gases can accumulate to potentially detectable atmospheric levels, shown through previous photochemical and spectral simulations that primarily assume terrestrial compositions (A. Segura et al. 2005; M. Leung et al. 2022; V. S. Meadows et al. 2023; D. Angerhausen et al. 2024).

Detection of methylated gases on Earth-like targets may require a larger investment in telescope time, but the low false-positive potential of these gases provides significant value from a potential observation, motivating them as spectral targets for follow-up observations. While proposed as potential

biosignatures on Hycean worlds (M. Leung et al. 2022; N. Madhusudhan et al. 2023a), these biogenic gases have not yet been evaluated using coupled photochemical and spectral simulations to quantify the detectability of biologically plausible production rates of methyl halides for Hycean planets. The extended hydrogen envelope of these planets will enhance feature size and potential detectability, increasing the biosignature detection potential on Hycean worlds. Here we use the methods developed in S.-M. Tsai et al. (2024) and applied to DMS in that work to explore methyl halides as biosignatures on Hycean exoplanets.

## 2. Methods

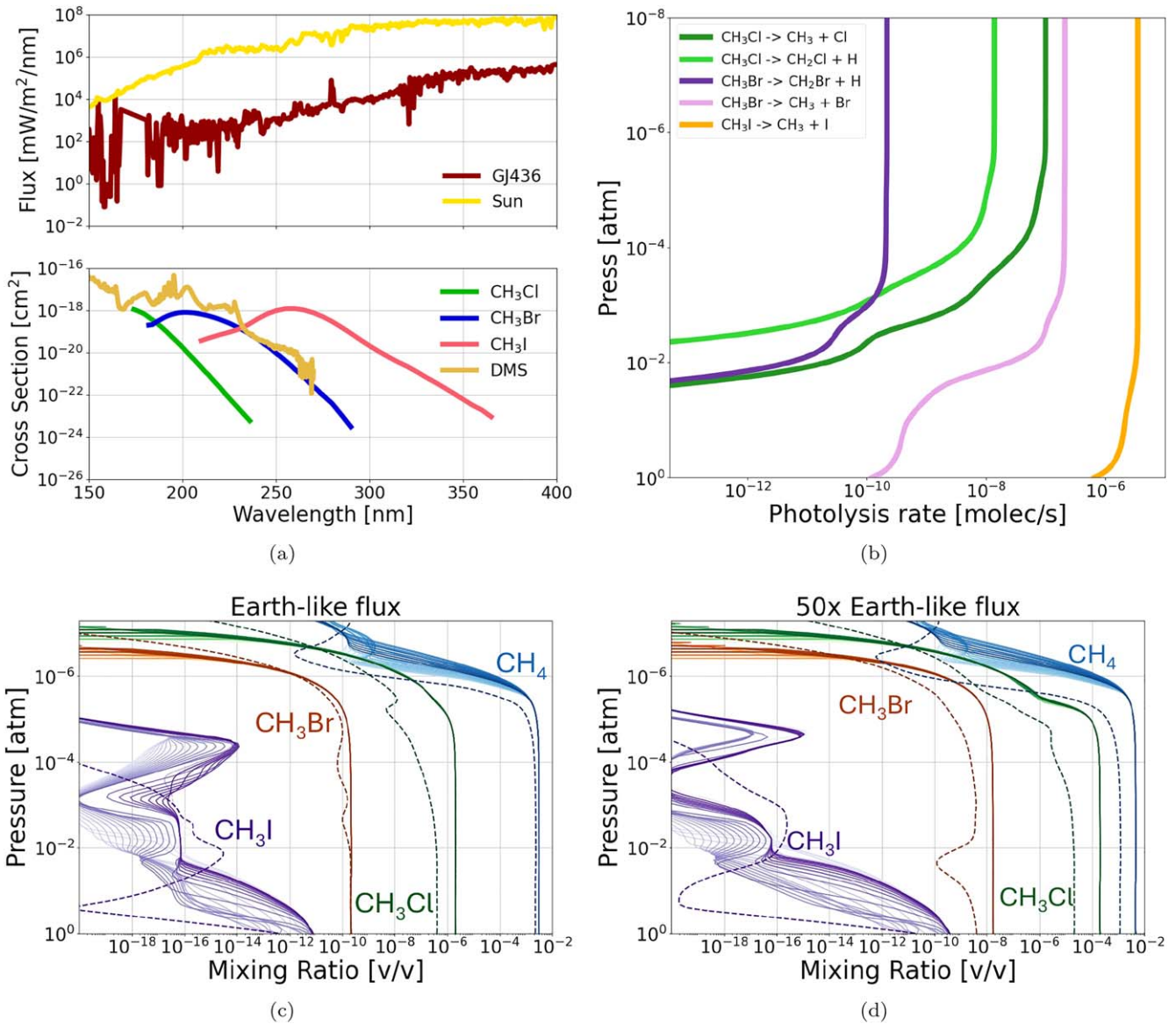
### 2.1. VULCAN Photochemical Model

We use the VULCAN photochemical code to model the potential accumulation of methyl halide biosignatures in Hycean atmospheres for a range of flux (surface production rate) conditions. VULCAN has been validated against a variety of planetary types including Earth, hot Jupiters, and temperate sub-Neptune planets (S.-M. Tsai et al. 2021a, 2021b; Z. Huang et al. 2024). We adopt the Hycean boundary conditions used in S.-M. Tsai et al. (2024), including the pressure–temperature profile generated for K2-18b. We utilize the same spectrum of GJ 436 and scaled solar spectra. For this study, we incorporate closed-loop reaction networks for methyl chloride ( $\text{CH}_3\text{Cl}$ ), methyl bromide ( $\text{CH}_3\text{Br}$ ), and methyl iodide ( $\text{CH}_3\text{I}$ ). This expansion totals 444 reactions, including 38 photodissociation reactions as well as the necessary thermodynamical data and photochemical cross sections. See Figure 1 for a comparison of the photochemical cross sections used here, alongside the stellar spectra. Cross-sectional data for  $(\text{CH}_3)_2\text{S}$  are also included for comparison to previous Hycean studies (i.e., S.-M. Tsai et al. 2024). We adopt the pressure–temperature profile from S.-M. Tsai et al. (2024) for a K2-18b-like Hycean planet without biological sources.

Building on the S–N–C–H–O photochemical network with DMS and DMDS in S.-M. Tsai et al. (2024), we extend the reaction network to incorporate closed-loop methyl halide reactions. The version of this code incorporating the halogen chemistry is available on Github<sup>5</sup>, and our full boundary conditions are reported in the Appendix. We adopt the methyl halide ( $\text{CH}_3\text{X}$ , X = Cl, Br, I) biogenic surface fluxes from M. Leung et al. (2022), with the addition of a  $\text{CH}_3\text{I}$  flux. We consider a range of gas fluxes up to 1000x the globally averaged flux on the Earth, a reasonable assumption given the known high spatial and temporal variability of the gas production (see M. Leung et al. 2022 for further discussion of highly productive organisms and environments). Marine ecosystems on Earth contribute to the global methyl halide flux (i.e., R. M. Moore 2003; X. Xiao et al. 2010), so global ocean environments such as Hycean worlds could plausibly yield biological production fluxes sufficient to generate atmospheric signals. Alternative evolutionary pathways could also lead to enhanced biosignature production on warm Hycean planets (E. G. Mitchell & N. Madhusudhan 2025).

Figures 1(c), (d) show the mixing ratio profiles, simulated using both 2D (S.-M. Tsai et al. 2024) and 1D photochemical models. The 2D results, shown in solid lines, shaded based on longitude, show moderate enhancements versus those modeled in 1D,

<sup>5</sup> <https://github.com/MichaelaLeung/VULCANCH3X>



**Figure 1.** (a) Comparison of stellar surface spectra for both the Sun and GJ 436, used here as a stand-in for K2-18, an M2.8V star (top), and photochemical cross sections for  $\text{CH}_3\text{X}$  gases and DMS (bottom). (b) Comparison of photolysis rates for  $\text{CH}_3\text{X}$  gases for Earth-like biological production flux levels simulated using K2-18b parameters. (c) Comparison of mixing ratio profiles for 1D (dashed) and 2D (solid, shaded by longitude) simulations using Earth-like flux levels. Modest enhancements of  $\text{CH}_3\text{Cl}$  are shown, with similar ratios of the other gases. The largest mixing ratio range is seen for  $\text{CH}_3\text{I}$ , which shows some longitudinal dependency. (d) Mixing ratios similar to (c) for  $50\times$  Earth-like flux, around where fluxes become potentially spectrally detectable. Enhancements of  $5\text{--}10\times$  are seen for all gases compared to 1D results.

especially for  $\text{CH}_3\text{Cl}$  and for the  $50\times$  biological production flux case. These results are consistent with S.-M. Tsai et al. (2024), finding that horizontal transport can oppose extreme nightside accumulation, though an enhancement of a factor of several is possible. This effect may mean that the 1D simulations explored in depth here underestimate the potential accumulation of these gases for tidally locked Hycean planets and that detection of methyl halides may be easier than our results suggest. To understand the difference in mixing ratios of  $\text{CH}_3\text{Cl}$ ,  $\text{CH}_3\text{Br}$ , and  $\text{CH}_3\text{I}$ , we compared the photolysis profiles generated from VULCAN. Figure 1(b) shows that, in addition to assumed lower surface biological fluxes, as shown in Table 1,  $\text{CH}_3\text{Br}$  and  $\text{CH}_3\text{I}$  are photolyzed much more rapidly than  $\text{CH}_3\text{Cl}$ , accounting for their lower relative enhancement in the simulated K2-18b atmosphere.

**Table 1**  
Globally Averaged Biological Surface Production Fluxes of Methyl Halides Included in This Study

Gas	Flux ( $\text{molec cm}^{-2} \text{ s}^{-1}$ )	Source
$\text{CH}_3\text{Br}$	$5.17 \times 10^6$	X. Yang et al. (2005)
$\text{CH}_3\text{Cl}$	$3.04 \times 10^8$	X. Xiao et al. (2010)
$\text{CH}_3\text{I}$	$5.51 \times 10^6$	F. Ziska et al. (2013)

**Note.** Values reported are from Earth science models for  $\text{CH}_3\text{Cl}$  and  $\text{CH}_3\text{Br}$  used to analyze the cycling of halogens, with high  $\text{CH}_3\text{Cl}$  values reflecting the elevated abundances of Cl compared to other halogens. The  $\text{CH}_3\text{I}$  data represent oceanic measurements on Earth and are extrapolated to a globally averaged local surface flux.

## 2.2. Planetary Spectrum Generator

To simulate the detection of methyl halide biosignatures, we use the Planetary Spectrum Generator (PSG; G. L. Villanueva et al. 2018, 2022) to model transmission and emission spectra based on the atmospheric composition, planetary, stellar, and observational parameters. PSG was originally developed by G. L. Villanueva et al. (2018) and has been used for a variety of solar system and exoplanet applications (i.e., D. Pidhorodetska et al. 2020; G. Suissa et al. 2020; G. Liuzzi et al. 2021; S. Ranjan et al. 2023; G. L. Villanueva et al. 2023; J. K. Eager-Nash et al. 2024). PSG uses correlated k-tables and, when necessary, line-by-line calculations to construct the atmospheric opacities. The input line lists for line-by-line calculations are from HITRAN and include measurements from  $3\ \mu\text{m}$  and longer wavelengths for methyl halides (I. E. Gordon et al. 2022). We simulate the noise reduction from multiple transits by dividing the noise by the square root of the number of transits being combined.

Here we use the NIRSpec PRISM and MIRI-LRS instrumental templates to simulate observations with JWST, including simulated multisource noise to determine the number of transits necessary to detect simulated features at  $3\sigma$  and  $5\sigma$  confidence. To calculate the signal-to-noise ratio (S/N), we determine the size of the feature by subtracting off the atmospheric continuum without the gas present. Then we use the simulated noise to find the S/N. We determine the number of transits necessary to detect the feature by dividing the desired confidence by the square root of the binned S/N as in D. Pidhorodetska et al. (2020). This method is common for first-pass observational analyses (i.e., J. Lustig-Yaeger et al. 2019; A. Bixel & D. Apai 2021; S.-M. Tsai et al. 2024) and has been shown to strongly correlate with retrieval-based calculations (D. Angerhausen et al. 2024). We bin the spectrum to  $R = 30$ .

## 3. Photochemical Results

The atmospheric accumulation of  $\text{CH}_3\text{Cl}$  in Hycean planets is a strong function of surface biological production flux, reaching parts-per-million levels for the M dwarf host case at modest fluxes of 1–20 times Earth’s global average and percent levels at the highest productivity scenarios (1000x Earth flux; comparable to those found in highly productive environments like salt marshes). The atmospheric buildup occurs at a greater than linear rate, with the mixing ratio increasing by two orders of magnitude when the biological production flux is increased one order of magnitude, from 10x Earth like to 100x Earth like. As expected, the accumulation potential for Sun-like hosts is smaller by about 2–3 orders of magnitude for each production rate scenario. This significant contrast is due to the reduced photolysis of methyl halides for M dwarf hosts. The reduction in photolysis rate is 4 orders of magnitude or greater for each methyl halide pathway. The effect of the stellar-driven photochemistry can be seen in Figure 2. Unlike the results of S.-M. Tsai et al. (2024) applied to DMS, we do not find a significant impact from methyl halide fluxes on CO or  $\text{C}_2\text{H}_6$  production. Methyl halides trend toward reformation (i.e.,  $\text{CH}_3 + \text{Cl} \rightarrow \text{CH}_3\text{Cl}$ ) after photolysis, whereas there are fewer known pathways for DMS to do the same, resulting in fewer downstream products from  $\text{CH}_3\text{X}$  destruction.

We also explore the impact of this planetary and stellar environment on other methyl halides.  $\text{CH}_3\text{Br}$  [ $\text{CH}_3\text{I}$ ] presents similar mixing ratios as recorded for modern Earth-like bulk atmospheres in M. Leung et al. (2022), reaching close to parts-per-million [10s of parts-per-trillion] levels for maximum productivity cases. The lower buildup of these

gases, in comparison to  $\text{CH}_3\text{Cl}$ , can be attributed to higher photolysis rates of these molecules in the absence of  $\text{O}_2/\text{O}_3$  shielding. Additionally, these gases have lower biological production fluxes on Earth, and their peak photodissociation wavelengths intersect with a higher flux part of an M dwarf spectrum (see Figure 1). For the simulations using the Sun as the host star, there is lower atmospheric accumulation due to the increased photolysis resulting from enhanced total UV flux.

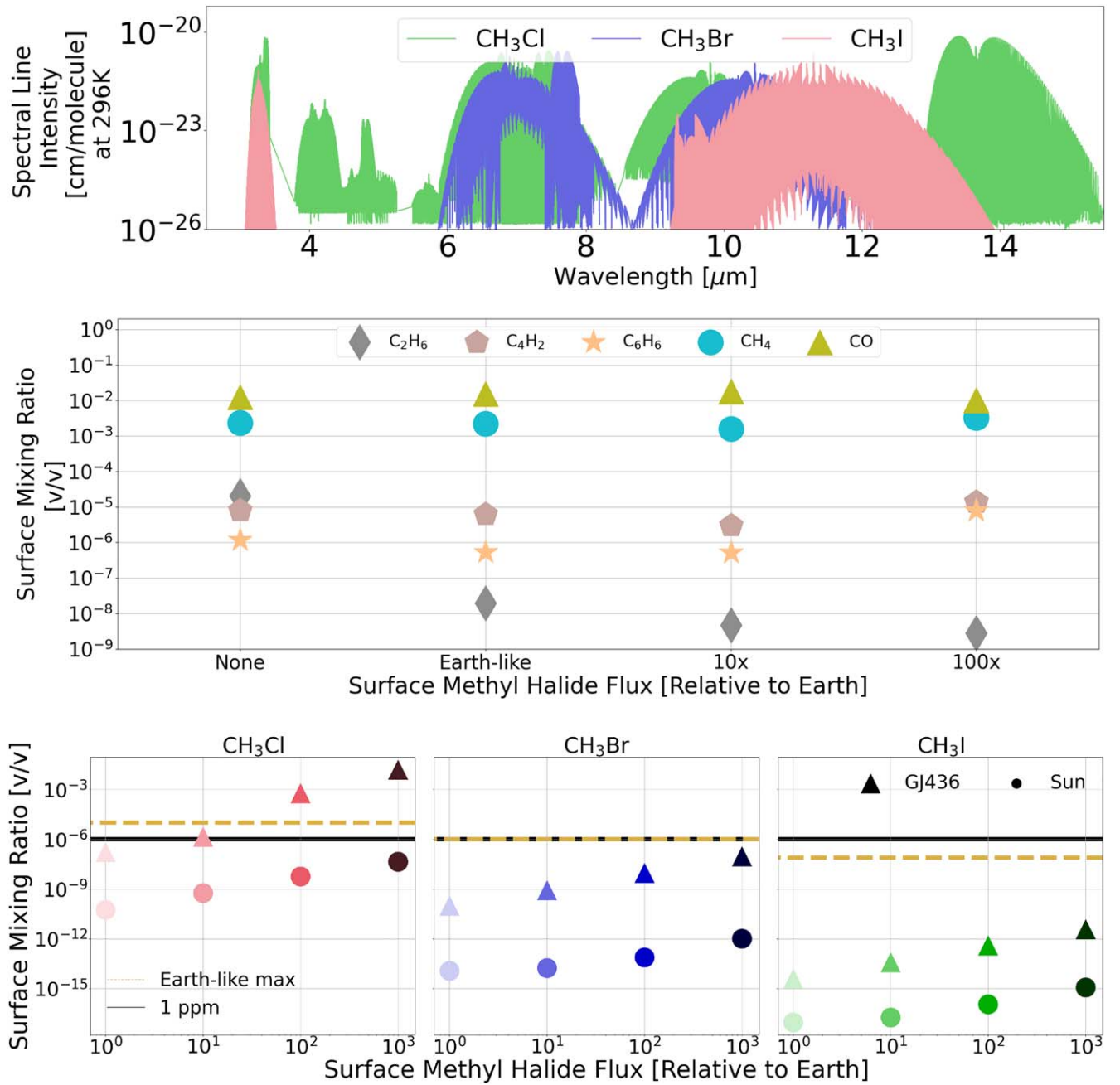
## 4. Atmospheric Detection

### 4.1. Using JWST

Simulated spectra including noise parameters for the NIRSpec PRISM and MIRI instruments suggest that detection of combined  $\text{CH}_3\text{X}$  features, for the range of surface biological production fluxes considered here, may be possible in 5–14 transits of K2-18b-like planets for optimistic biological production flux levels. We use the system and planetary parameters for K2-18b throughout the spectral simulations as a test case planet, including in transit. For the 1000x globally averaged Earth biological production flux cases, the high levels of accumulated  $\text{CH}_3\text{Cl}$  increase the mean molecular weight (MMW) of the atmosphere enough to change the overall continuum due to a reduction in scale height. Here, we focus on the flux cases (base, 10x, 100x), which maintain a MMW  $< 4$ , since the inflated light atmosphere lends an observational advantage to the planet. For the highest biological production flux case, the MMW increases to 4.5 from 3.9 with the base  $\text{CH}_3\text{X}$  flux. While our photochemical experiments consider all methyl halide gases, using those photochemical profiles to generate synthetic planetary spectra reveals that only  $\text{CH}_3\text{Cl}$  is sufficiently abundant to contribute atmospheric features for the flux cases considered here.  $\text{CH}_3\text{Br}$  and  $\text{CH}_3\text{I}$  opacities are considered in the radiative transfer model but in practice have no impact on the spectrum due to their low predicted abundance. Hereafter, we refer to the  $\text{CH}_3\text{Cl}$  spectral features only.

Figure 3 shows our simulated transmission spectroscopy observations, generated using PSG, for the NIRSpec PRISM instrument, suggesting that for the 100x [50x] globally averaged Earth biological production flux, it is possible to detect  $\text{CH}_3\text{Cl}$  at  $4.0\ \mu\text{m}$  with  $3\sigma$  confidence in 5 [12] transits of K2-18b. The other main “ $\text{CH}_3\text{X}$ ” feature in this area is also  $\text{CH}_3\text{Cl}$  at  $3.3\ \mu\text{m}$ ; however, this feature overlaps strongly with methane absorption features, so a diagnostic detection would be difficult, especially given the simultaneous elevated production of  $\text{CH}_4$  from the photochemical processing of  $\text{CH}_3\text{X}$  molecules. Other potential  $\text{CH}_3\text{X}$  features in this wavelength range are currently not quantitatively measured for  $\text{CH}_3\text{Br}$  and  $\text{CH}_3\text{I}$ .

In the mid-infrared, the  $\text{CH}_3\text{X}$  feature at  $10\ \mu\text{m}$ , also dominated by  $\text{CH}_3\text{Cl}$ , is the best candidate, requiring 26 transits for 100x biological production flux at a  $3\sigma$  detection level, calculated based on the MIRI-LRS instrument. There are  $\text{CH}_3\text{Br}$  and  $\text{CH}_3\text{I}$  features within this region, but sensitivity tests confirm that they do not generate detectable features for the conditions and parameters simulated in this work.  $\text{CH}_3\text{Cl}$  dominates the absorption features due to higher concentrations in the atmosphere. These detections of  $\text{CH}_3\text{Cl}$  would represent a considerable investment of telescope time; however, if other potential biosignatures had been detected on an exoplanet, searching for a capstone  $\text{CH}_3\text{Cl}$  signature in the mid-infrared may be justifiable and necessary to aid in interpretation.

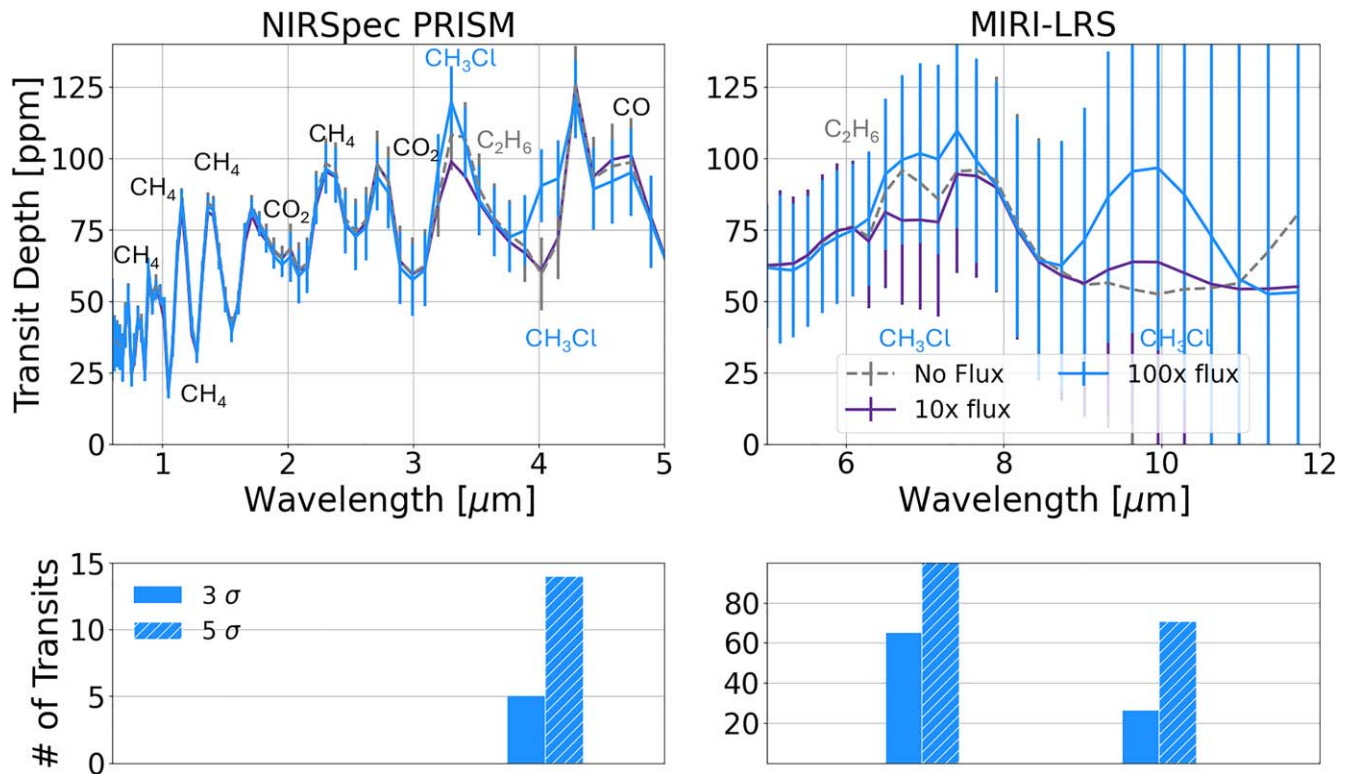


**Figure 2.** Top: methyl halide opacities used in spectral simulations. Data sourced from the HITRAN database (I. E. Gordon et al. 2022). Middle: comparison of haze precursor molecules in Hycean atmospheres for a variety of methyl halide flux levels. These gases are investigated here because S.-M. Tsai et al. (2024) showed that that CO and C<sub>2</sub>H<sub>6</sub> are highly responsive to DMS levels, with CO showing a large drop-off and C<sub>2</sub>H<sub>6</sub> a large increase as the organosulfur gas level increases. However, this trend does not hold here due to the rates of methyl halide reformation consuming the methyl radical and preventing further downstream chemical impacts. This is especially apparent in the large drop in C<sub>2</sub>H<sub>6</sub> levels between the “no methyl halide flux” case and the “Earth-like flux.” Bottom: comparison of average volume mixing ratios of methyl halide gases in Hycean-type atmospheres for the Sun and GJ 436, used here as a well-characterized test case for a relatively inactive M2 star like K2-18. The triangles show the GJ 436 stellar environment and circle markers the solar environment. The difference in accumulation level for CH<sub>3</sub>Cl is smaller in comparison to the other methyl halides because CH<sub>3</sub>Cl has less opacity in the near-UV and is less affected by the increased brightness of the Sun at these shorter wavelengths (see Figure 1). One part-per-million is shown with the black horizontal line as an approximate threshold for spectral relevance. Dashed yellow horizontal lines indicate mixing ratios reported for the most productive biological production flux scenario (1000x globally averaged) under modern Earth-like (O<sub>2</sub>-rich) bulk conditions in M. Leung et al. (2022) for CH<sub>3</sub>Cl and CH<sub>3</sub>Br. The same indicator for CH<sub>3</sub>I is from preliminary Earth-like photochemical simulations, provided here only as an estimate.

#### 4.2. Observability with the LIFE Telescope

These potential biosignature molecules are also accessible via emission spectroscopy. Our results for simulated Hycean worlds show that the absorption features of the methylated gases in emission are comparable to other features such as H<sub>2</sub>O and CO<sub>2</sub>. Figure 4 compares the impact of different CH<sub>3</sub>Cl biological

production flux levels on emission spectra for K2-18b. In addition to the major CH<sub>3</sub>Cl feature near 10  $\mu\text{m}$ , there is additional CH<sub>3</sub>Cl absorption between 6 and 8  $\mu\text{m}$  and longward centered at 13.7  $\mu\text{m}$ , also noted by S. Rugheimer et al. (2013) and M. Leung et al. (2022). Both features are dominated by CH<sub>3</sub>Cl, with minimal contributions by the other methyl halides.



**Figure 3.** Top left: simulated observations using JWST NIRSpec PRISM instrument. Optimal detection for  $\text{CH}_3\text{X}$  gases in 5 transits ( $3\sigma$ , 14 for  $5\sigma$ ) at the  $4.0 \mu\text{m}$   $\text{CH}_3\text{Cl}$  feature, which does not have strong  $\text{CH}_4$  interference, as seen for other  $\text{CH}_3\text{Cl}$  features in this spectral range (i.e.,  $3.3 \mu\text{m}$ ). Error bars are shown for 5 transits. Top right: simulated observations using JWST MIRI-LRS instrument. Both features are more difficult to detect due to instrumental constraints, but detection is possible for the  $10 \mu\text{m}$  band in tens of transits. For the “No Flux” scenario,  $\text{C}_2\text{H}_6$  features are present near  $3.3 \mu\text{m}$ , between  $6$  and  $8 \mu\text{m}$  and beyond  $12 \mu\text{m}$ , confounding the detection of methyl halide gases in these ranges. The presence of methyl halide gases at biological production levels appears to suppress  $\text{C}_2\text{H}_6$  abundances; see Section 5 for further discussion. Concentrations of other gases such as  $\text{CO}$  and  $\text{H}_2\text{CO}$  are also reduced when high levels of methyl radicals are introduced. Error bars shown are for 5 transits. Bottom: bar chart comparing number of transits necessary to detect each feature based on simulated noise for two confidence levels.

Following the same approach as in D. Angerhausen et al. (2023) and D. Angerhausen et al. (2024) we used LIFESIM (F. A. Dannert et al. 2022) to calculate the expected yields of K2-18b-like planets with LIFE and produce synthetic observations of the outlined exoplanet cases with different biological production flux levels of the discussed species and also without them being present in their atmospheres. For the presented output spectra, LIFESIM is configured with the current LIFE “baseline” setup (Quantum efficiency 0.7, Throughput 0.05, Wavelength 4–18.5  $\mu\text{m}$ , Spectral Resolution 50, Interferometric Baseline 10–100 m, Apertures Diameter 2 m, Exozodi 3x local zodi).

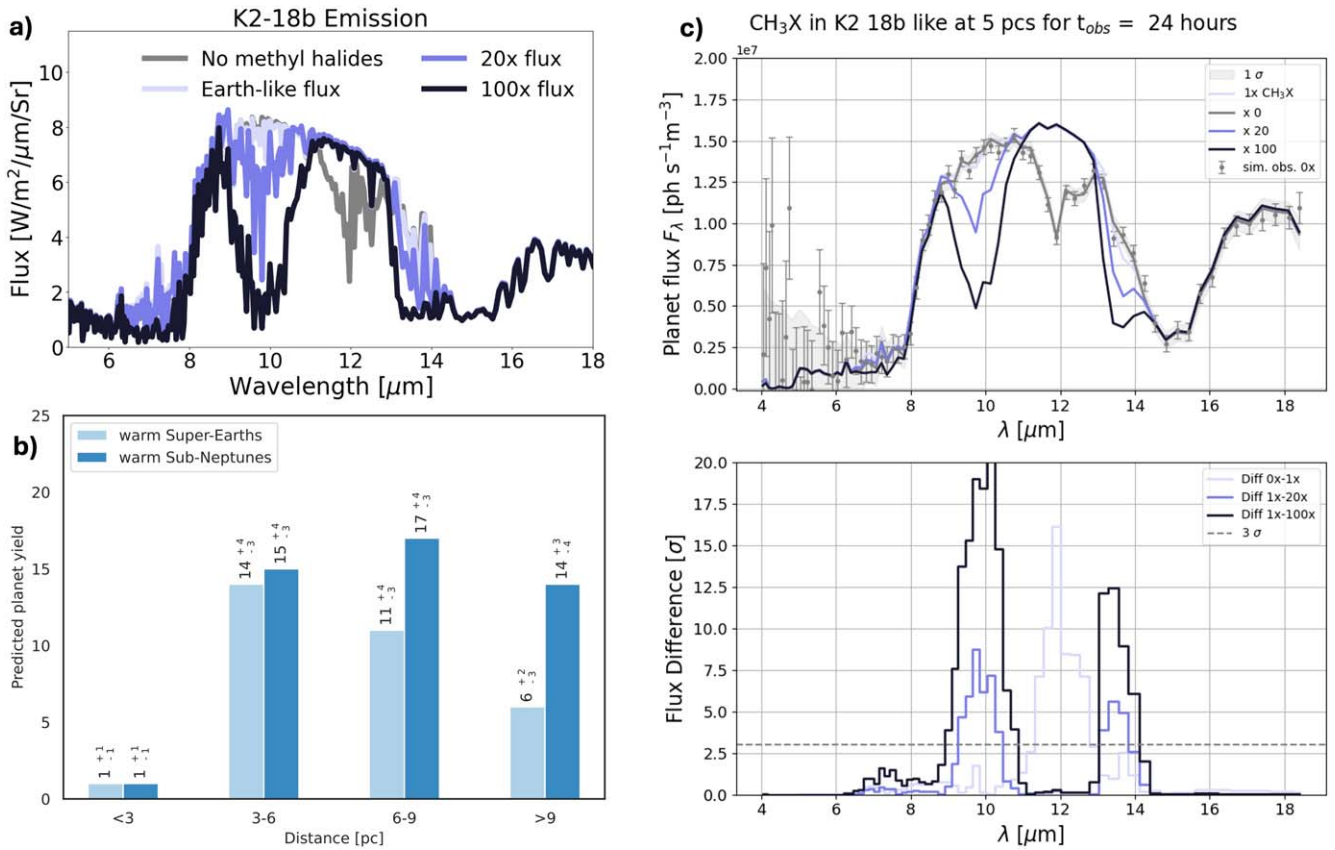
Our analysis (see Figure 4(b)) shows that LIFE will be able to detect more than 70 warm super-Earth and sub-Neptune planets within 10 pc. Based on this analysis, we choose 5 pc as a typical distance for our simulations presented here. LIFESIM simulations of the expected S/N (see Figure 4(c)) show that the various levels of  $\text{CH}_3\text{X}$  biological production fluxes discussed here will be detectable within only 24 hr of observations. This relatively small time requirement means that Hycean signals could be detected in the initial LIFE survey phase (i.e. S. P. Quanz et al. 2022) and may not require a dedicated characterization time to detect molecular features of methyl halides for these targets.

## 5. Discussion

The most favorable detection prospect for methylated gases in Hycean atmospheres would be under biological production flux conditions greater than 10x the globally averaged flux on the Earth, possibly through a greater radiation of the

methylation pathways or high productivity in the marine environment. The most favorable wavelength for current detection in transit is  $\sim 4.0 \mu\text{m}$ , where the NIRSpec PRISM instrument enables observations with lower noise. Our results suggest that to detect methylated gases on Hycean worlds with JWST requires a minimum of five transits, depending on the desired confidence level and observational wavelengths.

As of this writing, JWST is currently the most capable telescope to detect biosignatures on Hycean planets. However, NASA’s planned next flagship telescope, currently called the Habitable Worlds Observatory (HWO), will be optimized for searching for signs of life via reflected light spectroscopy on temperate planets orbiting nearby stars. This instrument is predicted to span UV, visible, and near-infrared (NIR) wavelengths up to  $2 \mu\text{m}$  only (National Academies of Sciences Engineering and Medicine 2023). This direction for biosignature science, in combination with the results presented here, motivates further exploration of methylated gas features at shorter NIR wavelengths ( $\lambda \leq 2 \mu\text{m}$ ). Shorter wavelength features for  $\text{CH}_4$  in the NIR and optical hint that additional methyl halide absorption features may also exist, but wavelength-specific opacities have not yet been measured at high fidelity. Further understanding of short wavelength  $\text{CH}_3\text{X}$  features through laboratory measurements is critical to constrain the applicability of these potential biosignatures to HWO. Complementarily, the LIFESIM results are highly favorable, showing that the time to detect  $\text{CH}_3\text{Cl}$  on a Hycean planet with thermal-IR emission spectroscopy is substantially lower than the time necessary to observe biosignature candidates



**Figure 4.** (a) Emission spectra of K2-18 b for various CH<sub>3</sub>X biological production flux levels using photochemical profiles as input. The largest feature can be seen at 10 μm, with smaller features appearing at 7 and 13.7 μm. (b) Distance distribution of warm sub-Neptunes and super-Earths around M- and FGK-type stars detectable with LIFE in the current baseline setup. For details on the exoplanet classification, see R. K. Kopparapu et al. (2018). The 5 pc distance assumed here is the typical distance for more than a dozen expected targets. (c) Detectability of various levels of CH<sub>3</sub>X (primarily CH<sub>3</sub>Cl) biological production fluxes in the emission spectrum of a “K2 18b-like” planet at 5 pc, after 24 hrs of observation with LIFE. Top: planetary emission for atmospheres with and without various levels of CH<sub>3</sub>Cl. The gray area represents the 1σ sensitivity; the gray error bars show an individual simulated observation. Bottom: statistical significance of the detected differences between atmospheric models with various levels of CH<sub>3</sub>X (see legend).

on a terrestrial world, further motivating this additional next-generation instrument (D. Angerhausen et al. 2024).

CH<sub>3</sub>Cl is the main contributor to CH<sub>3</sub>X features seen in this work, whereas in Earth-like (O<sub>2</sub>-rich) atmospheres, CH<sub>3</sub>Br can meaningfully contribute to the overall CH<sub>3</sub>X spectral features (M. Leung et al. 2022). Altitude-dependent photolysis of CH<sub>3</sub>X gases leads to this outcome, with photolysis of CH<sub>3</sub>Br and CH<sub>3</sub>I occurring much closer to the surface (i.e., Figure 1), resulting in both lower overall column densities and concentration of gases closer to the surface. Another reason that these molecules build up to lower levels is due to the lack of photochemical shielding, provided by O<sub>2</sub>/O<sub>3</sub> in an oxic environment. CH<sub>3</sub>Br and CH<sub>3</sub>I photolyze at longer wavelengths where the lack of shielding is more significant. Methyl halide gases are produced at different abundances based on the production environment (K. H. van Pée & S. Unversucht 2003); here we have used only the globally averaged ratios. In a global marine environment, the actual ratios may be different, and CH<sub>3</sub>Br or CH<sub>3</sub>I could emerge as the dominant methyl halide or provide a meaningful spectral contribution. We note that there are limited abiotic sources for CH<sub>3</sub>Cl and other methylated gases (i.e., E. C. Fayolle et al. 2017; N. Hänni et al. 2024; M. Sanz-Novo et al. 2025) but that the high destruction rates require a substantial source to overcome and reach detectable levels, unlikely to occur from modest abiotic sources (M. Leung et al. 2022).

Previous results have considered the role of DMS, also a methylated gas biosignature candidate in Hycean atmospheres (e.g., S.-M. Tsai et al. 2024). In comparison to DMS, all methyl halide gases considered here, CH<sub>3</sub>Cl, CH<sub>3</sub>Br, and CH<sub>3</sub>I, have more modest surface biological production fluxes (i.e., Table 1), which results in lower atmospheric accumulation, particularly for CH<sub>3</sub>Br and CH<sub>3</sub>I. We predict atmospheric accumulation of CH<sub>3</sub>Cl to similar levels as DMS, which is reasonable given the lower UV flux of the M2 host star at the relevant wavelengths for the CH<sub>3</sub>Cl cross section. Studies of DMS also demonstrated that high concentrations of CH<sub>4</sub> may obscure additional biosignature signals due to its strong opacity, particularly near 3.3 μm, and plausible high accumulation. This effect is reduced for this study due to the efficient reformation of methyl halides, allowing for optimal observations of CH<sub>3</sub>Cl at 4.0 μm.

Our results are based on the best available absorption cross-section measurements and spectral line list data. However, the necessary input absorption data have not been measured at high resolution or at all wavelengths relevant to exoplanetary studies. There is currently limited wavelength coverage for CH<sub>3</sub>Cl photodissociation data (J. B. Burkholder et al. 2020). If the cross section is larger than currently reported, there would be an increase in photolysis and decrease in mixing ratios. Constraining this uncertainty would enhance our confidence regarding the expected gas flux–abundance relationship of CH<sub>3</sub>Cl on Hycean planets.



In this work, we assume zero deposition velocity for  $\text{CH}_3\text{X}$  gases. In this scenario, surface sinks of the gases (i.e., biological consumption) are assumed to be at insignificant levels, and the gases would exist at saturation levels in the ocean. With higher deposition velocities, the atmospheric accumulation would decrease as surface sinks would take up the gas instead. This would rely on a biological process that can consume large amounts of methylated gases. Similarly to  $\text{CH}_4$ , while there is biological and surface uptake of  $\text{CH}_3\text{X}$  gases on Earth, the rates are vastly exceeded by the rate of production (R. C. Rhew & T. Abel 2007), in part due to modest water solubility for methyl halides. S.-M. Tsai et al. (2024) explore the impact of changing deposition velocity on atmospheric accumulation of DMS, finding that surface deposition is a limiting control on mixing ratio for this gas, a trend that would likely hold for the similarly behaved  $\text{CH}_3\text{X}$  gases.

Another factor not robustly explored here is the impact of the  $K_{zz}$  parameter. We assume a  $K_{zz}$  profile based on the Global Circulation Model simulations performed for S.-M. Tsai et al. (2024). Sensitivity tests suggest that higher  $K_{zz}$  values may contribute to more atmospheric accumulation of methylated gases in the upper atmosphere. These higher abundances would be easier to detect in spectral observations. Our  $K_{zz}$  values represent a conservative control on atmospheric accumulation where predicted detectability may be enhanced if eddy diffusion throughout the atmosphere is larger.

## 6. Conclusion

Building on previous work examining methylated gases as biosignatures for Earth-like planets, we consider their possible observability on potentially habitable sub-Neptune planets with a hydrogen envelope sitting over an ocean, creating conventionally habitable conditions. Atmospheric accumulation of  $\text{CH}_3\text{Cl}$  in this atmosphere type, simulated using K2-18b as a potential type case, shows that methylated gases (particularly  $\text{CH}_3\text{Cl}$ ) are well suited to build up in these environments and can easily reach parts-per-million levels and even percent levels for optimistic biological production flux assumptions. Spectral simulations reveal that these gas features are potentially detectable in as few as 14 transits using JWST instruments or 24 hr using next-generation space-based emission spectroscopy. These results support the use of methylated gases as corroborative “capstone” biosignatures in the near future, should any promising targets be revealed through preliminary characterization.

## Acknowledgments

This work was supported by the NASA Interdisciplinary Consortia for Astrobiology Research (ICAR) program via the CHAMPs (Consortium on Habitability and Atmospheres of M-dwarf Planets) team with funding issued under grant No. 80NSSC23K1399, the Alternative Earths team with funding issued under grant No. 80NSSC21K0594, and the Virtual Planetary Laboratory (VPL) team with funding issued under grant No. 80NSSC23K1398. Computations were performed using the computer clusters and data storage resources of the UCR HPCC, which were funded by grants from NSF (MRI-2215705, MRI-1429826) and NIH (1S10OD016290-01A1). M.L. thanks the UC President’s Dissertation Year Fellowship for partial funding for this work. The authors would also like to

thank Vincent Kofman for valuable comments concerning the noise modeling simulations.

*Software:* matplotlib<sup>6</sup> (J. D. Hunter 2007), numpy<sup>7</sup> (C. R. Harris et al. 2020), python<sup>8</sup> (G. Van Rossum & F. L. Drake 2009), Planetary Spectrum Generator<sup>9</sup> (G. L. Villanueva et al. 2018), VULCAN<sup>10</sup> (S.-M. Tsai et al. 2017, 2021b), spectres<sup>11</sup> (A. Carnall 2017). Software citation information aggregated using The Software Citation Station<sup>12</sup> (T. Wagg & F. S. Broekgaarden 2024; T. Wagg & F. Broekgaarden 2024).

## Appendix Photochemical Model Boundary Conditions

Our gas flux boundary conditions, including deposition velocities, are supplied for ease of replication in Table A1.

**Table A1**  
Boundary Conditions for Input in VULCAN Photochemical Model

Gas	Flux (molec cm <sup>-2</sup> s <sup>-1</sup> )	Deposition Velocity (cm s <sup>-1</sup> )
SO <sub>2</sub>	$9 \times 10^9$	1.0
H <sub>2</sub> S	$2 \times 10^8$	0.015
H <sub>2</sub> O <sub>2</sub>	0	1.0
S	0	1.0
SO	0	$3.0 \times 10^{-4}$
HSO	0	1.0
CH <sub>3</sub> S	0	0.01
COS	$5.4 \times 10^7$	0.003
CH <sub>3</sub> CH <sub>3</sub>	$4.2 \times 10^9$	0.0
CH <sub>3</sub> SH	$8.3 \times 10^8$	0.0
CS <sub>2</sub>	$1.4 \times 10^7$	0.0
CH <sub>4</sub>	$7.0 \times 10^{10}$	0.0
CH <sub>3</sub> Br	$5.17 \times 10^6$	0.0
CH <sub>3</sub> Cl	$3.04 \times 10^8$	0.0
CH <sub>3</sub> I	$5.51 \times 10^6$	0.0
ClO	0	0.5
HOCl	0	0.5
Cl <sub>2</sub>	0	1.0
ClONO <sub>2</sub>	0	0.5
CH <sub>2</sub> ClO <sub>2</sub>	0	1.0
HCl	$1.0 \times 10^8$	0.2
Cl	0	1.0
HClO <sub>4</sub>	0	0.2
Br	$1.51 \times 10^8$	1.0
BrO	0	0.5
HBr	$1.0 \times 10^6$	0.75
Br <sub>2</sub>	$7.59 \times 10^6$	0.01
HOBr	0	0.35
CH <sub>2</sub> Br	0	1.0
IO	$1.0 \times 10^7$	0.0
I <sub>2</sub>	0	1.0
HI	$3.2 \times 10^3$	0.0
CH <sub>3</sub> Cl	various	0.0
CH <sub>3</sub> Br	various	0.0
CH <sub>3</sub> I	various	0.0

<sup>6</sup> <https://matplotlib.org/>

<sup>7</sup> <https://numpy.org/>

<sup>8</sup> <https://www.python.org>



<sup>9</sup> <https://psg.gsfc.nasa.gov/>

<sup>10</sup> <https://github.com/exoclimate/VULCAN>

<sup>11</sup> <https://github.com/ACCarnall/spectres>

<sup>12</sup> <https://www.tomwagg.com/software-citation-station/>

## ORCID iDs

Michaela Leung  <https://orcid.org/0000-0003-1906-5093>  
 Shang-Min Tsai  <https://orcid.org/0000-0002-8163-4608>  
 Edward W. Schwieterman  <https://orcid.org/0000-0002-2949-2163>

Daniel Angerhausen  <https://orcid.org/0000-0001-6138-8633>

Janina Hansen  <https://orcid.org/0009-0003-1247-8378>

## References

- Angerhausen, D., Ottiger, M., Dannert, F., et al. 2023, *AsBio*, **23**, 183  
 Angerhausen, D., Pidhorodetska, D., et al. 2024, *AJ*, **167**, 128  
 Benneke, B., Roy, P.-A., Coulombe, L.-P., et al. 2024, arXiv:2403.03325  
 Benneke, B., Wong, I., Piaulet, C., et al. 2019, *ApJL*, **887**, L14  
 Bergsten, G. J., Pascucci, I., Mulders, G. D., Fernandes, R. B., & Koskinen, T. T. 2022, *AJ*, **164**, 190  
 Biagini, A., Cracchiolo, G., Petralia, A., et al. 2024, *MNRAS*, **530**, 1054  
 Bixel, A., & Apai, D. 2021, *AJ*, **161**, 228  
 Burkholder, J. B., Sander, S. P., Abbatt, J. P. D., et al. 2020, *Chemical Kinetics and Photochemical Data for Use in Atmospheric Studies Evaluation Number 19*, *Tech. Rep.* 19, Jet Propulsion Laboratory  
 Cabot, S. H. C., Madhusudhan, N., Constantinou, S., et al. 2024, *ApJL*, **966**, L10  
 Carnall, A. 2017, arXiv:1705.05165  
 Claudi, R., Alei, E., Battistuzzi, M., et al. 2020, *Life*, **11**, 10  
 Cooke, G. J., & Madhusudhan, N. 2024, *ApJ*, **977**, 209  
 Damiano, M., Bello-Arufe, A., Yang, J., & Hu, R. 2024, *ApJL*, **968**, L22  
 Dannert, F. A., Ottiger, M., Quanz, S. P., et al. 2022, *A&A*, **664**, A22  
 Dimmer, C. H., Simmonds, P. G., Nickless, G., & Bassford, M. R. 2001, *AtmEn*, **35**, 321  
 Domagal-Goldman, S. D., Meadows, V. S., Claire, M. W., & Kasting, J. F. 2011, *AsBio*, **11**, 419  
 Eager-Nash, J. K., Daines, S. J., McDermott, J. W., et al. 2024, *MNRAS*, **531**, 468  
 Fayolle, E. C., Öberg, K. I., Jørgensen, J. K., et al. 2017, *NatAs*, **1**, 703  
 Gordon, I. E., Rothman, L. S., Hargreaves, R., et al. 2022, *JQSRT*, **277**, 107949  
 Greiss, S., Steeghs, D., Gänsicke, B. T., et al. 2012a, *AJ*, **144**, 24  
 Greiss, S., Steeghs, D. T. H., Gänsicke, B. T., et al. 2012b, arXiv:1212.3613  
 Guerrero, N. M., Seager, S., Huang, C. X., et al. 2021, *ApJS*, **254**, 39  
 Hänni, N., Altwegg, K., Combi, M., et al. 2024, *ApJ*, **976**, 74  
 Harris, C. R., Millman, K. J., van der Walt, S. J., et al. 2020, *Natur*, **585**, 357  
 Holmberg, M., & Madhusudhan, N. 2024, *A&A*, **683**, L2  
 Hu, R., Beichman, C. A., Brain, D., et al. 2019, *BAAS*, **51**, 559  
 Hu, R., Damiano, M., Scheucher, M., et al. 2021, *ApJL*, **921**, L8  
 Huang, Z., Yu, X., Tsai, S.-M., et al. 2024, arXiv:2407.09009  
 Hunter, J. D. 2007, *CSE*, **9**, 90  
 Kopparapu, R. K., Hébrard, E., Belikov, R., et al. 2018, *ApJ*, **856**, 122  
 Leconte, J., Spiga, A., Clément, N., et al. 2024, *A&A*, **686**, A131  
 Leung, M., Schwieterman, E. W., Parenteau, M. N., & Faucher, T. J. 2022, *ApJ*, **938**, 6  
 Liuzzi, G., Villanueva, G. L., Viscardy, S., et al. 2021, *GeoRL*, **48**, e92650  
 Lustig-Yaeger, J., Meadows, V. S., & Lincowski, A. P. 2019, *AJ*, **158**, 27  
 Madhusudhan, N., Moses, J. I., Rigby, F., & Barrier, E. 2023a, *FaDi*, **245**, 80  
 Madhusudhan, N., Nixon, M. C., Welbanks, L., Piette, A. A. A., & Booth, R. A. 2020, *ApJL*, **891**, L7  
 Madhusudhan, N., Piette, A. A. A., & Constantinou, S. 2021, *AJ*, **918**, 1  
 Madhusudhan, N., Sarkar, S., Constantinou, S., et al. 2023b, *ApJL*, **956**, L13  
 Meadows, V. S., Lincowski, A. P., & Lustig-Yaeger, J. 2023, *PSJ*, **4**, 192  
 Mitchell, E. G., & Madhusudhan, N. 2025, *MNRAS*, *Advance Access*  
 Moore, R. M. 2003, *The Handbook of Environmental Chemistry* (Berlin: Springer), **85**  
 National Academies of Sciences Engineering and Medicine 2023, *Pathways to Discovery in Astronomy and Astrophysics for the 2020s* (Washington DC: The National Academies Press)  
 Pidhorodetska, D., Faucher, T., Villanueva, G., Domagal-Goldman, S., & Kopparapu, R. K. 2020, *ApJL*, **898**, L33  
 Pilcher, C. B. 2003, *AsBio*, **3**, 471  
 Quanz, S. P., Ottiger, M., Fontanet, E., et al. 2022, *A&AS*, **664**, A21  
 Ranjan, S., Schwieterman, E. W., Leung, M., Harman, C. E., & Hu, R. 2023, *ApJL*, **958**, L15  
 Redeker, K. R., Wang, N., Low, J. C., et al. 2000, *Sci*, **290**, 966  
 Rhew, R. C., & Abel, T. 2007, *EnST*, **41**, 7837  
 Rigby, F. E., & Madhusudhan, N. 2024, *MNRAS*, **529**, 409  
 Rivera, E. J., Lissauer, J. J., Paul Butler, R., et al. 2005, *ApJ*, **634**, 625  
 Rugheimer, S., Kaltenecker, L., Zsom, A., Segura, A., & Sasselov, D. 2013, *AsBio*, **13**, 251  
 Sanz-Novo, M., Rivilla, V., Endres, C. P., et al. 2025, *ApJL*, **980**, L37  
 Schwieterman, E. W., & Leung, M. 2024, *RvMG*, **90**, 465  
 Segura, A., Kasting, J. F., Meadows, V., et al. 2005, *AsBio*, **590**, 706  
 Sharma, S., Stello, D., Buder, S., et al. 2017, *MNRAS*, **473**, 2004  
 Shibazaki, A., Ambiru, K., Kurihara, M., Tamegai, H., & Hashimoto, S. 2016, *MarCh*, **181**, 44  
 Shorttle, O., Jordan, S., Nicholls, H., Lichtenberg, T., & Bower, D. J. 2024, *ApJL*, **962**, L8  
 Suissa, G., Mandell, A. M., Wolf, E. T., et al. 2020, *ApJ*, **891**, 58  
 Tsai, S.-M., Innes, H., Lichtenberg, T., et al. 2021a, *ApJL*, **922**, L27  
 Tsai, S.-M., Innes, H., Wogan, N. F., & Schwieterman, E. W. 2024, *ApJL*, **966**, L24  
 Tsai, S.-M., Lyons, J. R., Grosheintz, L., et al. 2017, *ApJS*, **228**, 20  
 Tsai, S.-M., Malik, M., Kitzmann, D., et al. 2021b, *ApJ*, **923**, 264  
 Tsai, S.-M., Parmentier, V., Mendonça, J. M., et al. 2024, *ApJ*, **963**, 41  
 Valencia, D., Sasselov, D. D., & O'Connell, R. J. 2007, *ApJ*, **656**, 545  
 van Pée, K. H., & Unversucht, S. 2003, *Chmsp*, **52**, 299  
 Van Rossum, G., & Drake, F. L. 2009, *Python 3 Reference Manual* (Scotts Valley, CA: CreateSpace)  
 Villanueva, G. L., Hammel, H. B., Milam, S. N., et al. 2023, *Sci*, **381**, 1305  
 Villanueva, G. L., Liuzzi, G., Faggi, S., et al. 2022, *Fundamentals of the Planetary Spectrum Generator* (Greenbelt, MD: Goddard Spaceflight Center)  
 Villanueva, G. L., Smith, M. D., Protopapa, S., Faggi, S., & Mandell, A. M. 2018, *JQSRT*, **217**, 86  
 von Bloh, W., Cuntz, M., Schröder, K.-P., Bounama, C., & Franck, S. 2009, *AsBio*, **9**, 593  
 Wagg, T., & Broekgaarden, F. 2024, *The Software Citation Station*, v1.0, Zenodo, doi:10.5281/zenodo.11292918  
 Wagg, T., & Broekgaarden, F. S. 2024, arXiv:2406.04405  
 Wogan, N. F., Batalha, N. E., Zahnle, K. J., et al. 2024, *ApJL*, **963**, L7  
 Xiao, X., Prinn, R. G., Fraser, P. J., et al. 2010, *ACP*, **10**, 5515  
 Yang, J., & Hu, R. 2024, *ApJ*, **971**, L48  
 Yang, X., Cox, R. A., Warwick, N. J., et al. 2005, *JGRD*, **110**, D23311  
 Yu, X., Moses, J. I., Fortney, J. J., & Zhang, X. 2021, *ApJ*, **914**, 38  
 Ziska, F., Quack, B., Abrahamsson, K., et al. 2013, *ACP*, **13**, 8915